Approximate Furrow Infiltration Model for Time-Variable Ponding Depth

E. Bautista, A.M.ASCE[1]; A. W. Warrick[2]; J. L. Schlegel[3]; K. R. Thorp[4]; and D. J. Hunsaker[5]

Abstract: A methodology is proposed for estimating furrow infiltration under time-variable ponding depth. The methodology approximates the solution to the two-dimensional Richards equation, and is a modification of a procedure that was originally proposed for computing infiltration under constant ponding depth. Two computational approaches were developed and tested using several combinations of soil hydraulic properties, furrow geometry, and flow depth variations. Both methods yielded solutions of reasonable and similar accuracy relative to numerical solutions of the two-dimensional Richards equation. The analysis also showed that the accuracy of the approximate model varies mostly as a function of soil hydraulic properties. The accuracy of the approximate solution can be improved with calibration. Two calibration methods were examined, one assuming that the calibration parameter varies with depth, and the other assuming a constant value. The analysis showed that latter approach, in combination with one of the proposed computational methods, reproduced the Richards equation solution more accurately. This means that a unique calibration parameter can be developed for the particular soil and geometric configuration conditions, and applied to different patterns of ponding depth variation. **DOI: 10.1061/(ASCE)IR.1943-4774.0001057.**

Introduction

The *WinSRFR* software package and other modeling tools for surface irrigation systems currently predict furrow infiltration using empirical formulations. The standard computational approach used by *WinSRFR* assumes that infiltration is given by a power law, dependent on infiltration opportunity time only and independent of flow depth and geometry. The software offers other alternatives, which assume that infiltration is still a function of opportunity time but proportional in some way to wetted perimeter. None of these methods account for the effect of pressure head on infiltration or initial soil water content (i.e., boundary and initial conditions). Empirical infiltration equations can be calibrated from field irrigation measurements and can probably generate reasonable infiltration and irrigation performance estimates if flow depths and opportunity times along the field are relatively uniform, such as with short furrows. However, opportunity times and flow depths tend to vary substantially along the run in long fields. Under those conditions, empirical furrow irrigation modeling is likely more unrealistic.

Several studies (e.g., Wohling et al. 2006; Banti et al. 2011) have proposed computing furrow infiltration in surface irrigation models using the two-dimensional Richards equation (Richards 1931; Warrick 2003). In the first author's opinion, such an approach is currently of limited value for practical irrigation studies, first because of the substantial computational time required by the numerical solution of the 2D Richards equation. More importantly, those coupled numerical solutions can exhibit convergence and mass balance problems. A computationally simpler and robust method is needed for practical studies, especially when considering that an irrigation analysis may potentially involve dozens or hundreds of simulations.

Warrick et al. (2007) proposed a furrow infiltration formulation based on approximate solution to the 2D Richards equation

$$\frac{I_{2D}(t)}{W^*} = I_{1D}(t) + \frac{\gamma S^2 t}{W \cdot (\theta_s - \theta_0)} \tag{1}$$

where I_{2D} = cumulative infiltration volume per unit length of furrow (L^2), calculated at a constant ponding depth h; I_{1D} = one-dimensional cumulative infiltration (L); t = time at which infiltration is calculated; γ = empirical parameter (−), calibrated from an infiltration time series simulated with the Richards equation; W^* = empirical adjusted wetted perimeter (L), calibrated from the same infiltration data as γ; W = wetted perimeter (L); θ_s and θ_0 = saturated and initial water content (−), respectively; and S = soil sorptivity ($L/T^{0.5}$).

Eq. (1) was derived from an expression developed for analyzing disk infiltrometer measurements (Smettem et al. 1994; Haverkamp et al. 1994) and later adapted to analyze infiltration from a strip source (Warrick and Lazarovitch 2007). The key premise behind all of these formulations is that for a given infiltration surface, the difference between infiltration volume per unit area and the corresponding one-dimensional infiltration [$I_{2D}/W^* - I_{1D}$ in the case of Eq. (1)], is a linear function of time. The difference, referred to as the edge effect (Warrick et al. 2007), corresponds to water that infiltrates primarily through the process of absorption. This concept is supported by experimental observations (Smettem et al. 1994) and also by comparison of simulated infiltration computed with the

[1]Research Hydraulic Engineer, U.S. Arid Land Agricultural Research Center, USDA-ARS, 21881N, Cardon Ln., Maricopa, AZ 85138 (corresponding author). E-mail: Eduardo.Bautista@ars.usda.gov

[2]Professor Emeritus, Dept. of Soil, Water and Environmental Sciences, Univ. of Arizona, Tucson, AZ 85721. E-mail: aww@cals.arizona.edu

[3]Information Technology Specialist, U.S. Arid Land Agricultural Research Center, USDA-ARS, 21881N, Cardon Ln., Maricopa, AZ 85138. E-mail: James.Schlegel@ars.usda.gov

[4]Research Agricultural Engineer, U.S. Arid Land Agricultural Research Center, USDA-ARS, 21881N, Cardon Ln., Maricopa, AZ 85138. E-mail: Kelly.Thorp@ars.usda.gov

[5]Research Agricultural Engineer, U.S. Arid Land Agricultural Research Center, USDA-ARS, 21881N, Cardon Ln., Maricopa, AZ 85138. E-mail: Doug.Hunsaker@ars.usda.gov

Note. This manuscript was submitted on September 28, 2015; approved on February 29, 2016; published online on June 8, 2016. Discussion period open until November 8, 2016; separate discussions must be submitted for individual papers. This paper is part of the ***Journal of Irrigation and Drainage Engineering***, © ASCE, ISSN 0733-9437.

two-dimensional and one-dimensional Richards equations (Warrick and Lazarovitch 2007; Warrick et al. 2007).

Warrick et al. (2007) noted that the ponding depth used for I_{1D} calculations, identified in this article as h_{1D}, must be less than h, because h varies along the wetted perimeter of the furrow. Hence, they set $h_{1D} = h_c$, where h_c is the center of mass of the flow cross section measured from the furrow bottom (h_c). The depth h_{1D} was also used to calculate soil sorptivity, using an expression developed for ponded water conditions (Haverkamp et al. 1988)

$$S = \sqrt{2K_s[\theta_s - \theta_0)(h_{1D} - h_f)]} \tag{2}$$

where K_s = saturated hydraulic conductivity [L/T]; and h_f = soil water pressure head at the wetting front [L]. If the $K(h)$ relationship for a soil is known, then h_f can be determined, as the hydraulic conductivity-weighted average of the soil water pressure head (Bouwer 1964)

$$h_f = \int_{h_0}^{0} \frac{K(h)}{K_s} dh \tag{3}$$

With this parameterization, Warrick et al. (2007) calibrated the parameters γ and W^* by fitting Eq. (1) to infiltration results generated with the *HYDRUS 2D/3D* program (Šejna et al. 2012). The $I_{1D}(t)$ contribution was calculated with *HYDRUS-1D* (Šimůnek et al. 2013). Simulations were conducted with different combinations of soil hydraulic properties [based on the van Genuchten (1980) soil hydraulic model], furrow flow depth, furrow geometry, the ratio of furrow depth to flow depth, and initial water content. Their analysis confirmed the linearity of the edge effect with time when calculated from simulated furrow irrigation data. The coefficient of determination of the linear regression line (R^2) computed for all of their tests was better than 0.998. For the range of conditions that they examined, they determined values for γ between 0.5–1.3, and between 0.8–1.3 for W^*/W.

Bautista et al. (2014b) compared simulated infiltration from furrows and strips, with the strip width equal to the furrow wetted perimeter. The ponding depth for the strip calculations was determined from the furrow ponding depth, using the centroid depth as in Warrick et al. (2007) but also using the wetted perimeter-averaged depth h_w

$$h_W = \frac{\int_W [h - \zeta(\chi)] ds}{\int_W ds} \tag{4}$$

In this expression, $\zeta(\chi)$ is the vertical coordinate of a point along the wetted perimeter as a function of the transverse coordinate χ. For a trapezoidal furrow with bottom width B_0 and side slope SS, the expression simplifies to

$$h_W = \frac{(h^2\sqrt{1 + SS^2} + hB_0)}{W} \tag{5}$$

with

$$W = 2h\sqrt{1 + SS^2} + B_0 \tag{6}$$

Furrow and strip calculations were in closer agreement when using h_w than with h_c. In view of these results, these authors simplified Eq. (1) by setting $W^* = W$ and conducted then additional calibration tests with $h_{1D} = h_w$. As with Warrick et al. (2007), γ varied with different soils and boundary conditions, but the range of variation was narrower for a given soil, especially when the absolute magnitude of h_f was large relative to h_W.

Eq. (1) was developed assuming a constant ponding depth h. However, in furrow irrigation systems h is a function of distance and time, i.e., at any particular location along the length of run, h rises from zero to a maximum value and gradually returns to zero. Hence, Bautista et al. (2014a) proposed a modification to Eq. (1), to account for time-variable ponding depth $h(t)$. That formulation generated reasonably accurate results under the limited set of soil and flow conditions under which it was tested. This study further examines this problem, proposes an alternative formulation, and examines the problem of calibrating the parameter γ under variable depth conditions.

Methodology

Approximate Solutions for Variable Ponding Depth

To facilitate the discussion, the approximate furrow infiltration model Eq. (1) is rewritten as

$$I_{2D}^i = Z_k^i + E_k^i \tag{7}$$

where Z denotes an estimator of the one-dimensional infiltration contribution; E = estimator of the edge effect ε; the superscript i = discrete time index; and the subscript k identifies a computational method. Several computational methods will be tested as part of this analysis. The edge effect is redefined as an infiltrated volume per unit length, i.e., as

$$\varepsilon_k^i = I_{2D}^i - Z_k^i \tag{8}$$

Hence, when h is fixed, and with the modifications proposed by Bautista et al. (2014b)

$$W^* = W \tag{9}$$

$$Z^i = Z_1^i = I_{1D}^i \cdot W \tag{10}$$

$$E^i = E_1^i = \frac{\gamma S^2 t^i}{(\theta_s - \theta_0)} \tag{11}$$

In what follows, computational method EZ1 will refer to the calculation of I_{2D} with Eqs. (10) and (11).

There are three difficulties in adapting Eqs. (10) and (11) to cases with time-dependent h. First, although a variable h can be easily incorporated into the calculation of I_{1D}, S, and W, the functions Z_1 and E_1, and therefore their sum, are guaranteed to increase monotonically with time only when h is constant or increasing. Thus, these functions need to be modified to ensure that the I_{2D} increases when h is decreasing.

Second, as was noted earlier, the linearity of the edge effect has been established for cases where h is constant. A variable h can be expected to make the edge effect less linear but the magnitude of that effect is unknown. This provides some flexibility in defining the Z_k function, but a matching E_k function must then be defined based on the same assumptions used to develop Z. One factor that was considered when examining alternatives for Z_k was its effect on the evolution of the edge effect relative to total infiltration, ε_R

$$\varepsilon_R = 1 - \frac{Z}{I_{2D}} \tag{12}$$

When h is constant, ε_R increases with time but levels off at long times. This follows from the derivative of Eq. (1)

$$\frac{d}{dt}\left(\frac{I_{2D}}{W^*}\right) = \frac{dI_{1D}}{dt} + \frac{\gamma S^2}{W \cdot (\theta_s - \theta_0)} \tag{13}$$

in which the first term gradually decreases (but converges to K_s for long times) while the second is constant. This development hypothesizes that ε_R evolves similarly when h is variable as when h is constant. This would seem a reasonable assumption, especially when h is decreasing with time, as those are conditions where the relative contribution of Z_k to total infiltration should decrease.

The last difficulty is the determination of γ. Prior results (Warrick et al. 2007; Bautista et al. 2014b) suggest that $\gamma(h)$ is an increasing function for small values of h, and then becomes relatively constant or may even decrease for larger values of h. If γ depends only on the particular depth at a given time, but is independent of the history of depth variations, then a $\gamma(h)$ function can be constructed for the particular soil, furrow geometry, and initial conditions, and then applied to hydrographs of any shape. Because $\gamma(h)$ tends to vary within a relatively narrow range, a constant value may suffice for practical calculations. This would greatly facilitate the calibration process not only from *HYDRUS 2D/3D* simulation results but also from field measured infiltration, a case in which γ would be subsumed in the value of K_s. However, if γ depends on the history of depth variations, i.e., if γ is unique to each particular $h(t)$ and is substantially different from values generated at constant h, then alternative calibration procedures need to be developed.

Two computational alternatives for handling time-variable h are proposed. The first, identified here as method ZE2, accounts for the changes in h and W during the time interval $\Delta t^i = t^i - t^{i-1}$ (Bautista et al. 2014a), where the superscript i is a discrete time index. These wetted perimeter changes are assumed to impact both Z and E. The Z component is calculated as

$$Z_2^i = Z_2^{i-1} + \Delta Z_2^i \tag{14}$$

in which

$$\Delta Z_2^i = \Delta I_{1D}^i \cdot W_a^i \tag{15}$$

$$\Delta I_{1D}^i = I_{1D}^i - I_{1D}^{i-1} \tag{16}$$

and

$$W_a^i = \frac{W^i + W^{i-1}}{2} \tag{17}$$

The upper boundary conditions used to calculate I_{1D} is the h_W time series calculated from the specified h time series. Likewise, W^i is a function of h^i and the furrow geometry.

The proposed expression for the edge effect, is

$$E_2^i = E_2^{i-1} + \Delta E_2^i \tag{18}$$

in which

$$\Delta E_2^i = \frac{\gamma (S_2^i)^2 \Delta t^i}{(\theta_s - \theta_0)} \frac{W_a^i}{W_r^i} \tag{19}$$

and

$$S_2^i = \sqrt{2K_s(h_{Wa}^i - hf)(\theta_s - \theta_0)} \tag{20}$$

In Eq. (19) the ratio of W_a^i to the running average of the wetted perimeter W_r^i is used to give greater weight to the edge effect contribution when W is increasing during a time step and less weight when W is decreasing. W_r^i is given by

$$W_r^i = \frac{1}{t_i} \int_0^{t_i} W dt \tag{21}$$

or for discrete time increments

$$W_r^i = \frac{1}{t_i} \sum_{k=1}^{i} W_a^k \cdot \Delta t_k \tag{22}$$

The S_2 term can be computed by averaging the h_w values over the time interval Δt_i, as done in Eq. (20) (with h_{Wa}^i the average value), or by averaging the S values. The resulting E values are essentially the same.

The previously described approach is guaranteed to produce a monotonically increasing infiltration function [because Eqs. (14) and (18) always result in positive values]. It yielded reasonably accurate results during initial testing (Bautista et al. 2014a), but problems were noted when applied to a wider range of examples. In some cases, the approximation initially underpredicts and later overpredicts the *HYDRUS 2D/3D* solution, or vice versa, and the errors are of similar magnitude. In those cases, calibration improves the accuracy of the approximation only slightly. Thus, a second alternative, identified as computational method ZE3, was developed.

That alternative uses running averages for the calculation of the Z_k and E_k terms and assumes $W^*/W = 1$, thus ignoring the effects of wetted perimeter variations on lateral infiltration. The Z_k term is calculated with

$$Z_3^i = I_{1D}^i \cdot W_r^i \tag{23}$$

This function can decrease with time when the water is receding because of the contribution of W_r. While this problem was not observed with any of the tests presented in this study, additional computational tests were conducted to identify conditions leading to that problem. Those tests revealed that the function Z_3 can decrease when $h(t)$ is strongly and positively skewed (the falling limb of the hydrograph extends over a much longer time than the rising limb). While such a hydrograph is unlikely to be observed under typical irrigation conditions, an error condition needs to be raised during execution if calculations are affected by declining Z_3 values.

Two separate expressions were developed for the calculation of E_k, the first of which is

$$E_3^i = \frac{\gamma (S_3^i)^2 t_i}{(\theta_s - \theta_0)} \tag{24}$$

in which sorptivity is calculated with a running average of h_W, h_{Wr}^i,

$$S_3^i = \sqrt{2K_s(h_{Wr}^i - h_f)(\theta_s - \theta_0)} \tag{25}$$

As with Eq. (23), the running average term, $h_{Wr}(t_i)$, can potentially lead to decreasing values when h is decreasing and the hydrograph is strongly skewed to the right. Nevertheless, and as will be shown later, this formulation in combination with Z_3, can produce some improvements relative to computational method ZE2 if γ is constant. However, it performs inadequately if used in combination with a depth-dependent γ. Hence, the following modified form of E_3 was also tested:

$$E_3(t_i) = E_3(t_{i-1}) + \Delta E_3(t_i) = E_3(t_{i-1}) + \frac{\gamma(h) S_3(t_i)^2 \Delta t_i}{(\theta_s - \theta_0)} \tag{26}$$

Hence, in the following analysis, the method ZE3 will refer to Eqs. (23) and (24) when using a constant γ, and Eqs. (23) and (26) when using a depth-dependent γ. Table 1 summarizes the equations used with all three proposed computational methods.

Table 1. Summary of Equations Used with Each Computational Method for Variable Ponding Depth

Computational method	Component	Equations
ZE1	Z_1	Eq. (10)
	E_1	Eq. (11)
ZE2	Z_2	Eqs. (14)–(16)
	E_2	Eqs. (18)–(20), and (21)
ZE3	Z_3	Eq. (23)
	E_3 (for constant γ)	Eqs. (24) and (25)
	E_3 (for depth dependent γ)	Eqs. (25) and (26)

Testing

The proposed formulations were evaluated using several combinations of soil hydraulic properties, furrow geometry, and ponding depth variations. Table 2 summarizes the soil hydraulic and furrow geometry characteristics of each scenario. The scenarios include soils described with the van Genuchten (vG) and the Brooks and Corey (1964) (BC) hydraulic models. For soils where the listed source is Rosetta, parameters were derived with the *Rosetta Lite* 1.1 program (Schaap 2003), using the soil textural class option. For those examples, a BC scenario was created for a texturally similar soil. Note that those scenarios, for example 2 and 3, do not correspond to the same soil. This is not the case for two sets of scenarios, 11, 12, and 13, 14. In those cases, the published vG parameters were converted to BC parameters using the approach of Morel-Seytoux et al. (1996). That method matches the wetting front pressure h_f of the original and converted hydraulic models. These scenarios were included to illustrate the effect of soil hydraulic model on the predicted infiltration and the resulting calibration parameter.

The soil parameters given in Table 2 are: θ_r = residual volumetric water content; θ_0 = initial water content; α = parameter of the water retention curve; n = parameter of the water retention curve; and θ_s, K_s, and h_f are as previously defined. The effect of geometry (identified in the table under the Geom column) was tested using only two configurations, a narrow (N) and a wide trapezoidal furrow (W). The bottom width (B_0) and side slope (SS) were set equal to, respectively, 0.15 m and 1.0 [H/V] for the narrow furrow, and 0.1 m and 2 for the wide furrow.

Each scenario of Table 2 was evaluated in combination with three ponding depth hydrographs, which were defined as follows. The approximate solution based on the computational method ZE2 (with $\gamma = 1$), was programmed into SRFR, the simulation engine of *WinSRFR*, but with the one-dimensional infiltration component calculated with the Green-Ampt formula (Green-Ampt 1911), modified to handle time-varying depth (Warrick et al. 2005). A *WinSRFR* simulation scenario was developed for each soil and geometry combination. The details of the length, slope, roughness, inflow rate, and cutoff time are not particularly important and are not given here. However, all simulations were conducted using a low gradient, blocked-end furrow, in order to produce substantial flow depths variations with distance and time. (With sloping-free draining furrows, near-normal depth generally is attained quickly). Moreover, for each irrigation simulation, the inflow rate and cutoff time were selected to produce an average infiltrated volume of 0.1 m^3/m (a 10 cm average infiltrated depth assuming a 1 m furrow spacing), but with some variation in the final infiltration distribution along the field. This limits the infiltration tests to volumes typically applied with furrow systems. Hydrograph sets similar to those shown in Fig. 1 were developed for each test. The figure shows the hydrograph computed at the upstream end (H1), the middle (H2), and the downstream end (H3) of the field for Test 1. With the last hydrograph, h never reaches a steady-state.

An exception to the previously described procedure were the hydrographs developed for scenarios 12 and 14. Because scenarios 11 and 12 represent in principle the same soil, the depth hydrographs developed for the vG scenario 11 were also used with scenario 12. Likewise, the depth hydrographs for the vG scenario 13 were used with the BC version of that test, scenario 14. As explained previously, of interest in this study is to compare simulated infiltration with the same soil but described with a different model, and subject to the same boundary conditions.

HYDRUS 2D/3D was used to generate the I_{2D} infiltration time series corresponding to each flow soil, geometry, and depth hydrograph combination. A 2 × 2 m computational domain was used for all simulations, with the finite-element size defined automatically by the software. A refinement was inserted on the furrow perimeter, again with the element size defined automatically. The number of nodes and finite elements was close to 2,100 and 4,100, respectively, with both geometries. All simulations used a variable head upper boundary condition, no flow on the sides, and free drainage at the lower boundary. A soil water tension of −1,000 cm was assumed as initial condition. ZE2 and ZE3 solutions were calculated for each of these tests, at selected values of time. The *HYDRUS 1D* software was used to calculate the I_{1D} infiltration series needed by the approximate solutions. These calculations used a 2 m computational domain, and a default discretization scheme (100 elements). More details about the *HYDRUS* setup are provided in Bautista et al. (2014b).

Table 2. Soil and Geometric Properties for the Test Scenarios

ID	Soil texture	Soil model	Source	θ_r (−)	θ_s (−)	α (1/cm)	n	K_s (cm/min)	h_f (cm)	Geom
S1	Casa Grande sandy loam	vG	Abbasi et al. (2004)	0.065	0.407	0.0689	1.3700	0.04	2.30	N
S2	Loamy sand	vG	vG-Rosetta	0.049	0.390	0.0347	1.7466	0.073	9.33	N
S3	Loamy sand	BC	Rawls et al. (1982)	0.035	0.437	0.1150	0.4740	0.10183	12.35	N
S4	Sandy clay	BC	Rawls et al. (1982)	0.109	0.430	0.0343	0.1680	0.002	48.43	W
S5	Sandy clay loam	vG	vG-Rosetta	0.063	0.384	0.0211	1.3298	0.00916	6.54	N
S6	Sandy clay loam	BC	Rawls et al. (1982)	0.068	0.398	0.0356	0.2500	0.00717	43.95	N
S7	Silty clay	vG	vG-Rosetta	0.111	0.481	0.0162	1.3207	0.00667	8.23	W
S8	Silty clay	BC	Rawls et al. (1982)	0.056	0.479	0.0292	0.1270	0.0015	58.91	W
S9	Silty clay loam	vG	vG-Rosetta	0.090	0.482	0.0084	1.5202	0.00772	27.55	N
S10	Silty clay loam	BC	Rawls et al. (1982)	0.040	0.471	0.0307	0.1510	0.0025	54.99	N
S11	Berino loamy fine sand	vG	Hills et al. (1991)	0.083	0.321	0.0182	1.5083	0.18833	12.43	N
S12	Berino loamy fine sand	BC	Hills et al. (1991)	0.083	0.321	0.1120	0.5083	0.18833	12.66	N
S13	Glendale clay loam	vG	Hills et al. (1989)	0.106	0.469	0.0104	1.3940	0.00912	16.44	W
S14	Glendale clay loam	BC	Hills et al. (1989)	0.106	0.469	0.0884	0.3940	0.00912	16.29	W

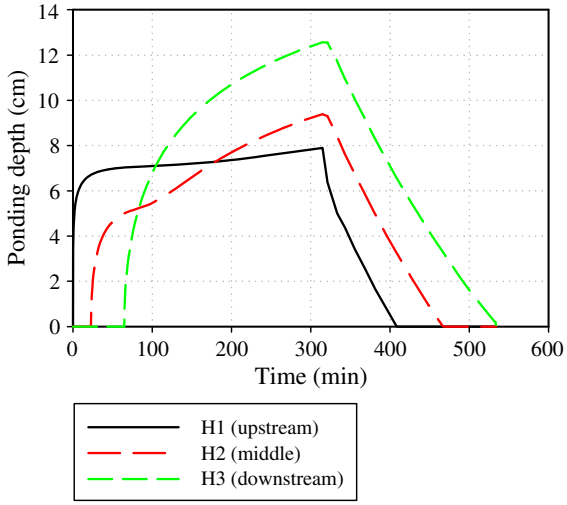

Fig. 1. Ponding depth hydrographs developed for scenario S1

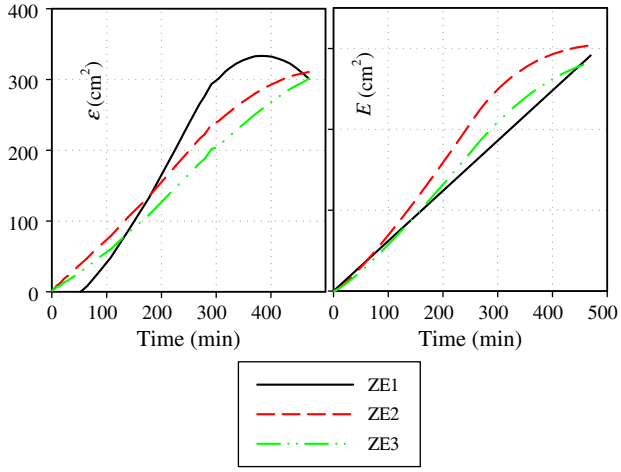

Fig. 3. Edge effect (ε) and estimator of the edge effect (E) computed for Example 2 (S1-H3)

Approximate solutions were compared with the I_{2D} simulation results, first with $\gamma = 1$, and later with calibrated γ values. Agreement between *HYDRUS 2D/3D* and approximate model results were evaluated using the root mean squared error (RMSE):

$$\text{RMSE} = \sqrt{\frac{\sum_{i=1}^{n} (O_i - P_i)^2}{m}} \tag{27}$$

where O represents an observation (in this case, a *HYDRUS 2D/3D* simulated value); P = predicted value (computed with method ZE2 or ZE3); and m = number of data pairs.

Results

Relationship between ε and E

Figs. 2 and 3 examine the effect of the Z2 and Z3 functions on the edge effect $\varepsilon = I_{2D} - Z$, and the relationship between ε and the corresponding uncalibrated ($\gamma = 1$) E functions. This analysis is performed using scenario S1 and two of the hydrographs from Fig. 1, H1 and H3. For comparison purposes, ε was calculated also

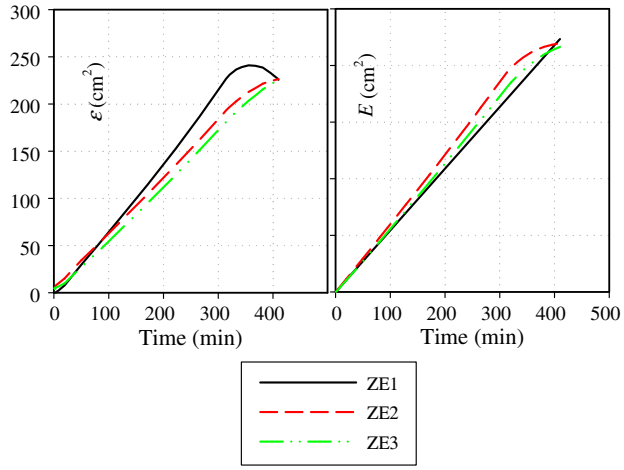

Fig. 2. Edge effect (ε) and estimator of the edge effect (E) computed for Example 1 (S1-H1)

with method ZE1. Hence, in that case the average h was used to calculate first I_{1D} and W in Eq. (10), and then the value of S required by Eq. (11). The left plot in each figure shows the time series $\varepsilon_1 = I_{2D} - Z_1$, $\varepsilon_2 = I_{2D} - Z_2$, and $\varepsilon_3 = I_{2D} - Z_3$ whereas the right plot illustrate the corresponding E functions. The linear regression coefficient of determination (R^2) for each series is given in Table 3. Also given in the table is the RMSE calculated between each ε and E pair (which is also the RMSE value computed between I_{2D} and $[Z + E]$).

As expected, Z_1 produced the most nonlinear ε functions and, consequently, the smallest R^2 and, consequently, the largest RMSE values. Z_2 and Z_3 linearized $\varepsilon(t)$ with both examples, more strongly with the latter method as can be observed in the graphs, although the R^2 was only slightly greater. The resulting RMSE values were less than 10 cm^2. As will be shown later, this is an exceptional group of tests as the RMSE for the uncalibrated function can be substantially greater for other soils.

Relative edge effect time series were computed with functions Z_2 and Z_3 (Fig. 4). They are identified in the figure as ε_{R2} and ε_{R3}, respectively, with the left hand side graph showing the results for the test with hydrograph H1 and the right with H3. The graph also shows the relative edge effect calculated using a constant h, ε_{R1}. In those cases, I_{2D} and I_{1D} were calculated with final average values of h and h_w, respectively (with Z_1 still computed using the average W). As was previously explained, because the derivative of E_1 is a constant, ε_{R1} gradually increases and levels off at very long times, as shown by corresponding plots. The ε_R series computed with Z_3 emulated this behavior more closely than the one computed with Z_2. In fact, when Z_2 was used for the computations, the slope of the ε_R function eventually changed sign, which is difficult to observe from the scale of the graph. These results could be interpreted as

Table 3. Performance of the Computational Methods ZE1, ZE2, and ZE3 for Tests S1-H1 and S1-H3

Test	Indicator	Computational method		
		ZE1	ZE2	ZE3
S1-H1	R^2	0.972	0.996	0.999
	RMSE (cm^2)	37.9	4.0	3.9
S1-H3	R^2	0.942	0.990	0.998
	RMSE (cm^2)	69.8	6.5	6.4

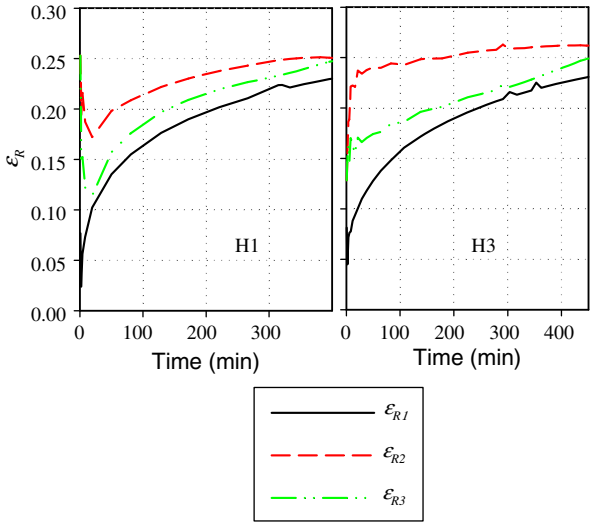

Fig. 4. Relative edge effect calculated for Examples 1 and 2

meaning that the edge effect is the same whether the ponding depth is constant or variable. If that is the case, then the function Z_3 should the preferred computational approach. However, both the Z_2 and Z_3 functions in combination with their corresponding E functions produced, ultimately, similar RMSE values. This could mean that the slope of the relative edge effect function is unimportant or could be just a characteristic of this particular group of tests. Of interest then is to determine if method ZE2 can produce an ε_R function that is even more negatively sloped under other soil, geometry, and boundary conditions, and if so, if that behavior compromises the accuracy of the calculations. The following section will present additional results to further examine this issue.

While method ZE1 generated the least accurate approximation, it can produce reasonable results under some conditions. For the test conducted with the H1 hydrograph, h attained near normal depth conditions in the first 25 min, rose again very gradually after 200 min due to backwater effects, and then dropped rapidly after cutoff. As a result, the average depth was nearly 80% of the peak value. This is reflected in the resulting ε function (Fig. 2, solid line), which varied near linearly until cutoff time, but became strongly nonlinear after that time. These results suggest that the ZE1 computational method, in combination with final average values for W and S, can deliver reasonable predictions with free-draining furrows on a relatively steep field-bottom slope. Those are conditions under which near steady-state flow would be achieved rapidly at any point along the furrow. It is important to note that even when producing reasonable results, use of method ZE2 or ZE3 would be preferable over ZE1 in combination with an irrigation simulation model. That is because latter method requires prior knowledge of the average final average depth as a function of distance down the field and that information is s an output of the simulation.

Performance of the Uncalibrated ZE2 and ZE3 Computational Methods

Fig. 5 is a boxplot of the computed RMSE values for all tests. The data are grouped by soil and computational method, with the ZE2 results displayed in white boxes and ZE3 results in gray boxes. Results are also grouped by soil hydraulic model, with vG soils (1, 2, 5, 7, 9, 11, 13) shown on the left half of the graph and BC soils (3, 4, 6, 8, 10, 12, 14) on the right. Clearly, soil is the factor that contributed the most to the variation in RMSE. Unlike the examples presented in the previous section where the RMSE were less than 10 cm^2 (1% of the target infiltration volume) for the tests associated with scenario S1, the average RMSE for all tests was 30 cm^2 and was as large as 90 cm^2 for soil S13. Tests conducted with different hydrographs for each soil produced, mostly, similar RMSEs. Likewise, for each individual test (soil and hydrograph combination), the two computational methods produced RMSEs of similar magnitude. Results do not suggest that one method is consistently more accurate than the other, as RMSEs computed with method ZE2 were greater than those computed with ZE3 for some soils, but smaller for other soils. The average RMSE for each computational method is shown in the figure legend in parentheses.

The *lme4* library (Bates et al. 2015a) of the R statistical software package (R Core Team 2015) was used to conduct a linear mixed model analysis of the RMSE values. The primary objective was to confirm that RMSE values are not affected by the computational method, i.e., that both computational methods, without calibration, yield equally accurate results. A secondary objective was to evaluate the contribution of the various factors considered in this

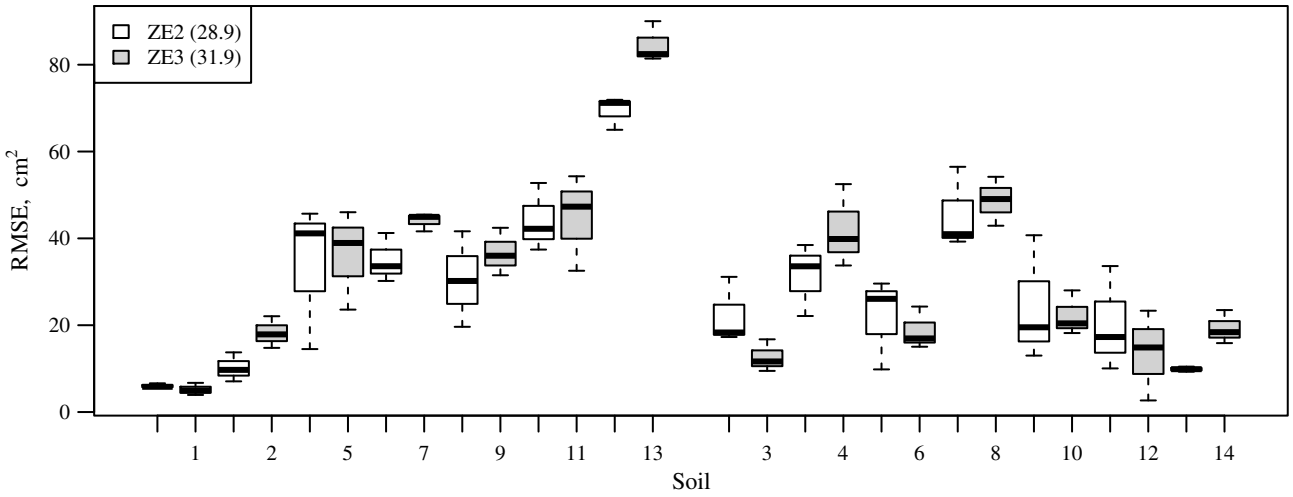

Fig. 5. Boxplot of RMSE values computed with the uncalibrated computational methods. van Genuchten soils are shown on the left and Brooks-Corey soils on the right side of the graph

Table 4. Linear Mixed Analysis for RMSE Values Computed with the Uncalibrated ZE2 and ZE3 Computational Methods: Random Effects

Groups	SD (cm^2)
Soil	14.97
Hyd	3.05
Residual	7.72

analysis to the performance of the approximate furrow infiltration model. Because many soil (*Soil*) and hydrograph (*Hyd*) scenarios are possible, these factors were treated as random effects. In principle, many furrow geometry (*FG*) configurations are possible but the analysis was limited to only two shapes, thus this factor was treated as a fixed effect, as were soil hydraulic model (*SHM*), and computational method (*CM*). The analysis assumed a random intercept with fixed mean for each random factor. Using the R software notation, the statistical model is

$$\text{RMSE} \sim SHM + CM + FG + (1/Soil) + (1/Hyd) + e \quad (28)$$

where e is the error term.

Tables 4–6 present the linear mixed model analysis results. Soil explains much of the variation in RMSE values (Table 4). The standard deviation (SD) associated with the soil factor was about twice the SD associated with the residuals while the SD of the hydrograph factor was less than half. In Table 5, the fixed factor analysis, the column labeled *Estimate* gives the intercept of the linear model and the slope for each of the fixed factors. Because the factors are categorical, the slope is the change in RMSE between categories for that factor. The largest change in RMSE was due to furrow geometry, which is indicated by the notation FGW, which implies that the intercept is associated with the narrow furrow category and that the slope represents the change from the narrow to the wide category. For this factor, RMSE increased by 21.7 cm^2 with wide furrows in comparison with narrow ones. In contrast, the RMSE changed the least due to computational method, on average a 3 cm^2 increase with method ZE3 relative to ZE2 as indicated by the line CMZE3 (which implies that the intercept applies to the computational method ZE2).

The statistical significance of the fixed factors was evaluated using the likelihood ratio test (Pinheiro and Bates 2000; Bates et al. 2015b), which consists of an analysis of variance that compares a proposed statistical model [in this case, the model represented by Eq. (28)] against a reduced version of that model [i.e., Eq. (28) without one of the *SHM*, *CM*, or *FG* factors]. The ANOVA function of the *lme4* library was used for this analysis. This test has one degree of freedom, which is the difference in the number of statistical parameters estimated with each model. The Chi-square distribution statistic (χ^2) and probability level (p) computed for each of three tests are summarized in Table 6. Because the comparison of the full model with a model that excluded the *CM* factor produced a nonsignificant difference, [$\chi^2(1) = 3.14$, $p = 0.076$], one can conclude that the *CM* factor has a nonsignificant impact on the RMSE

Table 5. Linear Mixed Model Analysis for RMSE Values Computed with the Uncalibrated ZE2 and ZE3 Computational Methods: Fixed Effects

Factor	Estimate (cm^2)	Standard error (cm^2)
Intercept	14.41	7.14
*SHM*_vG	13.51	8.27
*CM*_ZE3	3.02	1.70
*FG*_W	21.66	8.63

Table 6. Linear Mixed Model Analysis for RMSE Values Computed with the Uncalibrated ZE2 and ZE3 Computational Methods: Statistical Significance of Fixed Factors

Excluded factor	Chi sq.	Pr (> Chi sq.)
SHM	3.003	0.083
CM	3.140	0.076
FG	6.272	0.012[a]

[a]Statistically significant.

values. The only fixed factor that produced a significant difference was *FG* [$\chi^2(1) = 6.27$, $p = 0.012$]. Overall, results mean that without calibration, the proposed approximate model infiltration represents van Genuchten and Brooks-Corey soils with similar accuracy, independently of the computational method, but that predictions are more accurate for the narrow than the wide furrow used in these tests.

$\varepsilon_R(t)$ relationships were developed for all of these examples (not illustrated). In all cases, method ZE3 produced a more linear relationship than method ZE2, while the latter method occasionally produced relationships with a negative slopes, as in Fig. 4. Nevertheless, and as shown by Fig. 5 and the results of the statistical analysis, both methods ultimately yielded solutions of similar accuracy. Hence, computational inadequacies of the Z_2 function, if any, are being compensated by the E_2 function.

As was mentioned earlier, method ZE3 was developed after noting that in some cases method ZE2 slightly underpredicts at short times, and overpredicts as time increases, and that under those conditions, calibration may not improve results much. In those cases method ZE3 tends to shift the infiltration curve upward, and make the error negative at both short and long times. This effect is illustrated with Fig. 6. The left-hand side plot compares the *HYDRUS* and ZE2 solutions computed for test S7-H3, while the right compares the *HYDRUS* and ZE3 solutions for the same test. While this shifting of the curve increases the magnitude of errors at long times prior to calibration, it improves the accuracy of predictions with ZE3 in comparison with ZE2 after calibration, as will be demonstrated in the following section.

Scenarios S11 and S12 represent the same soil, as do scenarios S13 and S14. As explained in the "Methodology" section, these pairs of scenarios were included to compare infiltration computed with the Richards equation and with the approximate model under

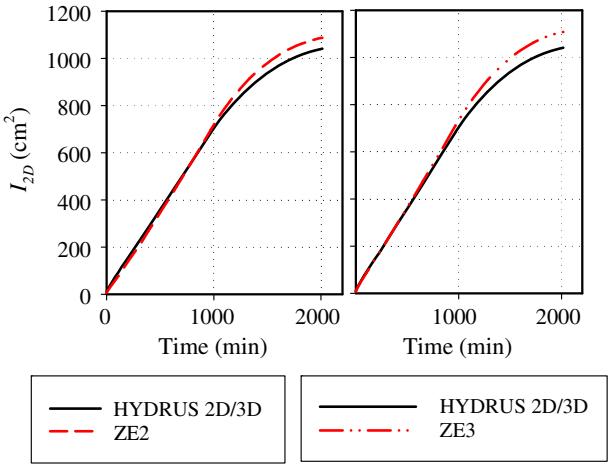

Fig. 6. Comparison of the *HYDRUS 2D/3D* and approximate model solutions

the same conditions. In both cases, larger RMSE values were calculated when using vG model than with the BC model. This is in contrast with the results of the mixed model analysis which indicated no difference on average between RMSE values computed with for vG and BC soils. In principle, the conversion formulas of Morel-Seytoux et al. (1996) make the solutions to the Richards equation in combination with the vG model similar to solutions generated in combination with the BC model at low water tensions. Solutions differ, substantially for some soils, because water tension varies discontinuously at low tensions with the BC model, but continuously with the vG model. In addition, if the initial condition is given as a tension, as done in this study, the initial water will likely not match. Predictions with the approximate model differ solely as a result of the difference in θ_0 because the conversion formulas yield the same capillary drive h_f for the a soil described with either the vG or BC model. The key point of this discussion is that the assumed soil hydraulic model will affect the performance of the uncalibrated approximate model for a particular soil, and that the resulting calibration parameters will be specific to that soil and model.

Performance with Calibrated Values of γ

Two different approaches were tested for calibrating γ, in both cases assuming that γ is independent of $h(t)$. The first approach, labeled G1, was to develop a $\gamma(h)$ function for constant values of h. For each soil-geometry scenario, I_{2D} time series were simulated with *HYDRUS 2D/3D* at selected values of h. All simulations were conducted for the same infiltration opportunity time, and thus involved different infiltration amounts. Approximate infiltration results were then computed with method ZE1 for the same depths. The approximate results were then fitted to the I_{2D} series using least-squares and an optimization routine. In the second approach, labeled G2, a constant γ was derived from one of the I_{2D} series simulated with variable depth for each soil-geometry scenario. In all cases, the downstream hydrograph developed for each scenario was used for calibration (e.g., H3 in Fig. 1), as that curve varied the most with time. As with the first method, least-squares and optimization were used to fit the approximate solution to the I_{2D} time series. Separate values of γ were computed for the ZE2 and ZE3 computational methods.

The $\gamma(h)$ functions computed for these sets of tests (Fig. 7, solid symbols) exhibited mostly similar patterns and ranges of variations as those presented by Bautista et al. (2014b). Exceptions were BC scenarios 3 and 12, where γ generally exceeded unity in the range of depths considered. Both cases involve light soils. For other tests, $\gamma(h)$ varied between 0.6 and 1.0, with results suggesting slightly smaller values for vG soils than for BC soils, and also larger values for lighter soils and smaller ones for heavier ones. Note that not all of the $\gamma(h)$ functions varied smoothly, for example the functions computed for Scenarios 1 and 7. This scatter is believed to be related to numerical artifacts of both the *HYDRUS 2D/3D* and *HYDRUS 1D* simulations.

Fig. 7 also displays the γ values derived from a single infiltration test with variable ponding depth. Values derived with the ZE2 computational method are shown as open circles and values derived with ZE3 are represented as open triangles. These results, plotted at the average value of h, were close to the values computed with the first calibration procedure. Exceptions were Scenarios 7, 10, and particularly 12. Again, these differences are believed to be related to numerical artifacts. γ values derived with both computational methods were, generally, in close agreement. A noticeable exception was Scenario 7, which as was noted earlier, exhibited other anomalies.

Infiltration was computed for each scenario and hydrograph test using methods ZE2 and ZE3, first in combination with the $\gamma(h)$ function and then using only the constant γ. The latter results include the test used for calibration. The resulting RMSE values are summarized again with a boxplot (Fig. 8), with results grouped first by soil and then by the combined computational-calibration method (e.g., ZE2G1), identified in what follows simply as computational method. As in Fig. 5, vG soils are on the left of the graph and BC soils on the right. RMSE were substantially smaller for these tests than for those of Fig. 5. Still, results varied substantially among soils. More importantly, results suggest differences among computational methods. The average RMSE for each method, is shown in the legend.

The RMSE values were analyzed using, again, linear mixed model procedures and the statistical model Eq. (28) (Tables 7–9). Calibration reduced the contribution of both random effects, soil and hydrograph (Table 7). Hence, and in contrast with the results of Table 4, the SD of soil for the calibrated computational methods was about two-thirds of the value for the residuals while the SD of hydrographs was only about one-tenth. Likewise, calibration generally reduced the differences between categories of each fixed factor (Table 8 versus Table 5), as indicated by the absolute magnitude of the estimated slopes. The exception was method ZE3G2, which reduced the RMSE by 8.4 cm^2 in relation to method ZE2G1. This supports the earlier observation of potential differences in RMSE values computed as a function of the *CM* factor.

Such differences were examined, first, using the likelihood ratio test. As before, the analysis involves comparing Eq. (28) with a simpler model that excludes a fixed factor, one at a time. *CM* (computational method) was the only factor that produced significant differences [$\chi^2(3) = 32.29,\ p = 4.55$ E-07] (Table 9). Given this result, a multiple comparison test was conducted to determine the significance of differences among computational methods. Bates (2010) outlines several procedures that can be followed to make such multiple comparisons. In cases involving a single fixed and random factor, one approach is to treat the random factor as a fixed factor, i.e., as a blocking factor. A conventional analysis of variance, in combination with a comparison of treatments using Tukey's method, is used in that case. However, application of such an approach would require eliminating hydrographs as a random variable from the analysis. A test was conducted to compare of Eq. (28) against a model that used soil as the only random factor and computational method as the only fixed factor. The test produced a nonsignificant difference, meaning that the variation in RMSE values can be explained by soil and computational method alone. Hence, an analysis of variance was conducted using the analysis-of-variance function of R, *aov*, using soil as a blocking factor (Bates 2010). These results were then used to compare the four computational methods using Tukey's significant difference method, as implemented in R. This procedure calculates the 95% confidence interval for all comparisons. That interval is given as Lower and Upper Bound in Table 10. An interval containing zero implies a nonsignificant difference. Because all comparisons involving method ZE3G2 do not contain zero, those differences are significant.

Overall, these results show that the approximate model can match the *HYDRUS 2D/3D* predictions with excellent accuracy, if properly calibrated, but that the accuracy of results will vary depending on soil and calibration method. Of the four combinations of computational and calibration method, ZE3G2 yielded the closest approximation to the *HYDRUS 2D/3D* results, with an average RMSE of 7.4 cm^2. Results indicate that whether using method ZE2 or ZE3, γ can be calibrated using a representative hydrograph

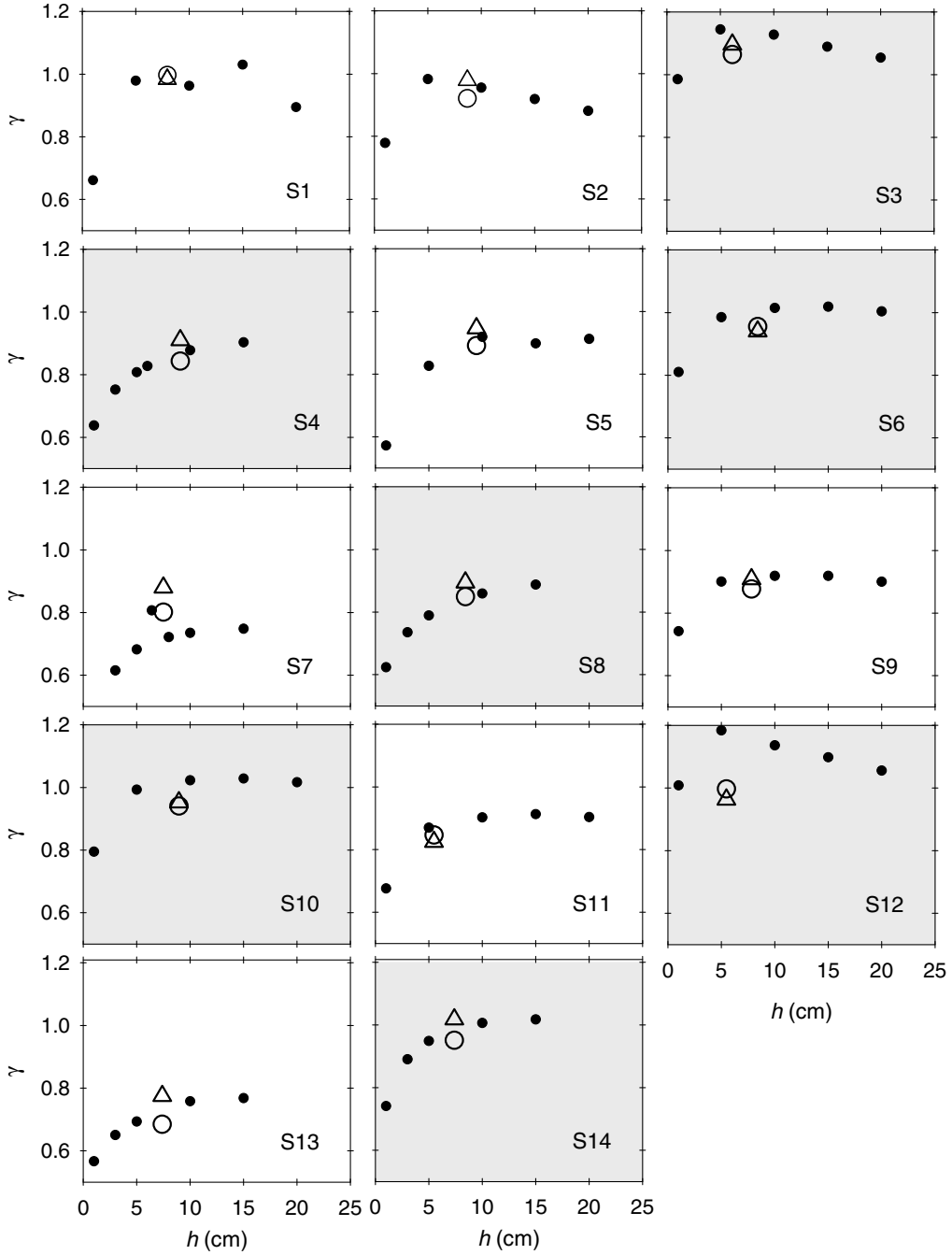

Fig. 7. $\gamma(h)$ functions developed at constant values of h (solid symbols), and γ values developed from a hydrograph with variable h (open symbols)

with variable depth (G2), under the assumption that such a value is constant for the expected range of depth variations.

Discussion

An important challenge to the use of the approximate furrow infiltration model will be the source of the soil hydraulic data. Two categories of data sources can be considered. In one case, the data will come from published reports, pedotransfer functions, or laboratory measurements. In those cases, the user will likely expect the approximate model to replicate as closely as possible the solution obtained with the two-dimensional Richards equation. Calibration will be needed to ensure the accuracy of predictions for the particular soil and geometric configuration. Under these conditions, the recommended computational approach is using ZE3 [Eqs. (23)–(25)].

Because soil hydraulic data are difficult to measure and validate at the scale of a field, a more likely scenario is that the parameters will be fitted from irrigation evaluation data, as is currently done with empirical infiltration formulations. Because the analysis of the previous section has shown that a constant γ can be assumed for particular soil and geometry conditions, and range of ponding depth variations, no special procedures will be needed to determine γ. That parameter will be embedded in the value of the estimated parameters, most likely in the value of K_s. Under these conditions,

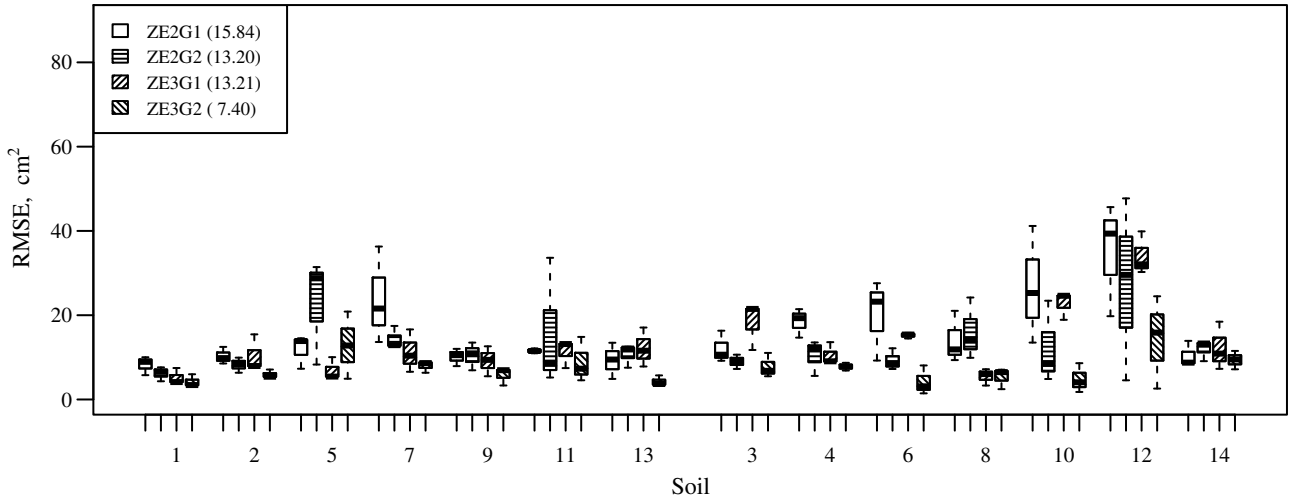

Fig. 8. Boxplot of RMSE values computed with the calibrated computational methods. van Genuchten soils are shown on the left and Brooks-Corey soils on the right side of the graph

Table 7. Linear Mixed Analysis for RMSE Values Computed with the Calibrated ZE2 and ZE3 Computational Methods: Random Effects

Groups	SD (cm^2)
Soil	4.495
Hyd	0.761
Residual	6.732

Table 8. Linear Mixed Analysis for RMSE Values Computed with the Calibrated ZE2 and ZE3 Computational Methods: Fixed Effects

Factor	Estimate (cm^2)	Standard error (cm^2)
Intercept	18.94	2.42
*SHM*_vG	−4.45	2.65
*CM*_ZE2G2	−2.65	1.47
*CM*_ZE3G1	−2.63	1.47
*CM*_ZE3G2	−8.44	1.47
*FG*_W	−2.44	2.76

Table 9. Linear Mixed Model Analysis for RMSE Values Computed with the Calibrated ZE2 and ZE3 Computational Methods: Statistical Significance of Fixed Factors

Excluded factor	Chi-sq.	Pr (>Chi sq.)
SHM	3.178	0.075
CM	32.287	4.550×10^{-7}[a]
FG	0.951	0.330

[a]Statistically significant.

Table 10. Results of Tukey's Significant Difference Test for Differences between Calibrated Computational Methods

Comparison	Difference (cm^2)	Lower bound (cm^2)	Upper bound (cm^2)	p adj
ZE2G2-ZE2G1	−2.646	−6.480	1.189	0.2809
ZE3G1-ZE2G1	−2.627	−6.462	1.207	0.2870
ZE3G2-ZE2G1	−8.439	−12.273	−4.604	0.0001
ZE3G1-ZE2G2	0.018	−3.816	3.853	1.0000
ZE3G2-ZE2G2	−5.793	−9.627	−1.958	0.0008
ZE3G2-ZE3G1	−5.811	−9.646	−1.977	0.0007

there is probably no reason to recommend method ZE3 over ZE2 [Eqs. (14)–(20)], especially because the latter is guaranteed to produce a monotnically increasing infiltration function.

There are other features that need to be added to the model to make it more generally useful. An important limitation of physically-based infiltration models is their ability to properly represent the initial wetting, when infiltration may be dominated by flow through cracks and macropores. This near-instantaneous infiltration causes the infiltration function versus time function to exhibit very rapid changes in slope at short times, which cannot be adequately described by the Richards equation (or the Green-Ampt model, if using a semiempirical modeling approach). Several empirical or semiempirical approaches have been proposed for dealing with this initial infiltration (Corwin et al. 1991; Ahuja et al. 1993; Clemmens and Bautista 2009). The model does not currently account for variations in texture along the soil profile or for merging wetting bulbs of neighboring furrows. These issues require further investigation.

Conclusions

The approximate furrow infiltration formulation of Warrick et al. (2007) has been modified to account for time-variable pressure (flow depth) at the infiltrating surface. Two numerical formulations were tested along with two methods for deriving the calibration parameter. The modified equation matches infiltration predicted with the two-dimensional Richards equation with reasonable accuracy, especially when using a formulation that incorporates wetted perimeter and flow depth effects using running averages in combination with a calibration parameter derived from a representative hydrograph with variable ponding depth. Results indicate that the calibration parameter γ under variable ponding depth is of similar magnitude as the value derived assuming a constant flow depth. Given the potential uncertainty in determining this parameter under variable depth conditions, the predicted performance of furrow irrigation systems does not appear to be critically sensitive to this parameter, especially when considering the uncertainty of other inputs.

Notation

The following symbols are used in this paper:

B_0 = furrow bottom width (L);
E = estimator of the edge effect ε;
h = water ponding depth (water pressure at the soil surface) (L);
h_{1D} = ponding depth used for I_{1D} calculations;
h_f = soil water pressure head at the wetting front (L);
h_W = wetted perimeter averaged depth (L);
h_{Wr} = running average wetted perimeter averaged depth;
I_{1D} = cumulative one-dimensional cumulative infiltration (L);
I_{2D} = cumulative infiltration volume per unit length of furrow (L^2);
$K(h)$ = hydraulic conductivity (L/T);
K_s = saturated hydraulic conductivity (L/T);
S = soil sorptivity ($L/T^{0.5}$);
SS = furrow side slope (L/L);
t = time at which infiltration is calculated (T);
W = wetted perimeter (L);
W^* = empirical adjusted wetted perimeter;
W_a = wetted perimeter averaged over a time step;
W_r = running average of the wetted perimeter;
Z = estimator of the one-dimensional infiltration contribution to I_{2D};
γ = empirical parameter (−);
ε = edge effect, the difference between I2D and Z;
ε_r = relative edge effect;
θ_0 = initial water content (−); and
θ_S = saturated water content (−).

References

Abbasi, F., Feyen, J., and van Genuchten, M. T. (2004). "Two-dimensional simulation of water flow and solute transport below furrows: Model calibration and validation." *J. Hydrol.*, 290(1–2), 63–79.

Ahuja, L., DeCoursey, D. G., Barnes, B. B., and Rojas, K. W. (1993). "Characteristics of macropore transport studied with the ARS rot zone water quality model." *Trans. ASAE*, 36(2), 369–380.

Banti, M., Zissis, T., and Anastasiadou-Partheniou, E. (2011). "Furrow irrigation advance simulation using a surface-subsurface interaction model." *J. Irrig. Drain. Eng.*, 10.1061/(ASCE)IR.1943-4774.0000293, 304–314.

Bates, D. (2010). "Lme4: Mixed-effects modeling with R." ⟨http://lme4.r-forge.r-project.org/lMMwR/lrgprt.pdf⟩.

Bates, D., Maechler, M., Bolker, B., and Walker, S. (2015a). "lme4: Linear mixed-effects models using Eigen and S4." ⟨http://CRAN.R-project.org/package=lme4⟩.

Bates, D., Maechler, M., Bolker, B. M., and Walker, S. (2015b). "Fitting linear mixed-effects models using lme4." *J. Stat. Software*, 67(1), in press.

Bautista, E., Warrick, A. W., and Schlegel, J. L. (2014a). "Wetted-perimeter dependent furrow infiltration and its implication for the hydraulic analysis of furrow irrigation systems." *Proc., World Environmental and Water Resources Congress 2014*, W. C. Huber, ed., ASCE-EWRI, Reston, VA, 1727–1735.

Bautista, E., Warrick, A. W., and Strelkoff, T. S. (2014b). "New results for an approximate method for calculating two-dimensional furrow infiltration." *J. Irrig. Drain. Eng.*, 140(10), 04014032.

Bouwer, H. (1964). "Unsaturated flow in ground-water hydraulics." *J. Hydraul. Div.*, 90(HY5), 121–144.

Brooks, R. H., and Corey, A. T. (1964). *Hydraulic properties of porous media*, Colorado State Univ., Fort Collins, CO.

Clemmens, A. J., and Bautista, E. (2009). "Toward physically based estimation of surface irrigation infiltration." *J. Irrig. Drain. Eng.*, 10.1061/(ASCE)IR.1943-4774.0000092, 588–596.

Corwin, D. L., Waggoner, B. L., and Rhoades, J. D. (1991). "A function model of solute transport that accounts for bypass." *J. Environ. Qual.*, 20(3), 647–658.

Green, W. H., and Ampt, G. A. (1911). "Studies on soil physics: I. Flow of air and water through soils." *J. Agric. Sci.*, 4(1), 1–24.

Haverkamp, R., Kutilek, M., Parlange, J. Y., Rendon, L., and Krejca, M. (1988). "Infiltration under ponded conditions: 2. Infiltration equations tested for parameter time-dependence and predictive use." *Soil Sci.*, 145(5), 317–329.

Haverkamp, R., Ross, P. J., Smettem, P. J., and Parlange, J. Y. (1994). "Three dimensional analysis of infiltration from the disc infiltrometer: 2. Physically based infiltration equation." *Water Resour. Res.*, 30(11), 2931–2935.

Hills, R. G., Porro, I., Hudson, D. B., and Wierenga, P. J. (1989). "Modeling one-dimensional infiltration into very dry soils. 1. Model development and evaluation." *Wat. Res. Res.*, 25(6), 1259–1269.

Hills, R. G., Wierenga, P. J., Hudson, D. B., and Kirkland, M. R. (1991). "The second Las Cruces trench experiment: Experimental results and two-dimensional flow predictions." *Water Res. Res.*, 27(10), 2707–2718.

HYDRUS [Computer software]. Microsoft, Redmond, WA.

Morel-Seytoux, H. J., Meyer, P. D., Nachabe, M., Touma, J., and van Genuchten, M. T., and Lenhard, R. J. (1996). "Parameter equivalence for Brooks-Corey and van Genuchten soil characteristics: Preserving the effective capillary drive." *Water Resour. Res.*, 32(5), 1251–1258.

Pinheiro, J. C., and Bates, D. M. (2000). *Mixed-effects models in S and S-Plus*, Springer, New York.

Rawls, W. J., Brakensiek, D. L., and Saxton, K. E. (1982). "Estimation of soil water properties." *Trans. ASAE*, 25(5), 1316–1320.

R Core Team. (2015). *R: A language and environment for statistical computing*, R Foundation for Statistical Computing, Vienna, Austria.

Richards, L. A. (1931). "Capillary conduction of liquids through porous mediums." *Physics*, 1(5), 318–333.

Schaap, M. (2003). "Rosetta Lite Version 1.1." USDA-ARS George E. Brown Jr. Salinity Laboratory and Univ. of California Riverside, Dept. of Environmental Sciences, Riverside, CA.

Šejna, M., Šimůnek, J., and van Genuchten, M. T. (2012). *The HYDRUS software package for simulating the two- and three-dimensional movement of water, heat, and multiple solutes in variably-saturated media user manual version 2.02*, PC-Progress, Prague, Czech Republic.

Šimůnek, J., Šejna, M., Saito, H., Sakai, M., and van Genuchten, M. T. (2013). "The HYDRUS-1D software package for simulating the one-dimensional movement of water, heat, and multiple solutes in variably-saturated media. Version 4.16." Dept. of Environmental Sciences, Univ. of California Riverside, Riverside, CA.

Smettem, K. R. J., Parlange, J. Y., Ross, P. J., and Haverkamp, R. (1994). "Three-dimensional analysis of infiltration from the disc infiltrometer. 1. A capillary-based theory." *Water Res. Res.*, 30(11), 2925–2929.

van Genuchten, M. T. (1980). "A closed-form equation for predicting the hydraulic conductivity of unsaturated soils." *Soil Sci. Soc. Am. J.*, 44(5), 892–898.

Warrick, A. (2003). *Soil water dynamics*, Oxford University Press, New York.

Warrick, A. W., and Lazarovitch, N. (2007). "Infiltration from a strip source." *Water Resour. Res.*, 43(3), W03420.

Warrick, A. W., Lazarovitch, N., Furman, A., and Zerihun, D. (2007). "Explicit infiltration function for furrows." *J. Irrig. Drain. Eng.*, 10.1061/(ASCE)0733-9437(2007)133:4(307), 307–313.

Warrick, A. W., Zerihun, D., Sanchez, C. A., and Furman, A. (2005). "Infiltration under variable ponding depths of water." *J. Irrig. Drain. Eng.*, 10.1061/(ASCE)0733-9437(2005)131:4(358), 358–363.

WinSRFR [Computer software]. USDA, Washington, DC.

Wöhling, T., Fröhner, A., Schmitz, G. H., and Liedl, R. (2006). "Efficient solution of the coupled one-dimensional surface—Two-dimensional subsurface flow during furrow irrigation advance." *J. Irrig. Drain. Eng.*, 10.1061/(ASCE)0733-9437(2006)132:4(380), 380–388.